Available online at www.sciencedirect.com
SCIENCE DIRECT
Polymer 46 (2005) 4421–4430
polymer
www.elsevier.com/locate/polymer

Hexadecyl-functionalized lamellar mesostructured silicates and aluminosilicates designed for polymer–clay nanocomposites. Part I. Clay synthesis and structure

Thuy T. Chastek[a], Emily L. Que[a], Jay S. Shore[c], Robert J. Lowy III[a], Christopher Macosko[b], Andreas Stein[a,*]

[a]Department of Chemistry, University of Minnesota, 207 Pleasant St SE, Minneapolis, MN 55455, USA
[b]Department of Chemical Engineering and Materials Science, University of Minnesota, 421 Washington Ave. SE, Minneapolis, MN 55455, USA
[c]Department of Chemistry and Biochemistry, South Dakota State University, Brookings, SD 57007, USA

Available online 15 April 2005

Abstract

Motivated by a need for synthetic clays that can be dispersed and exfoliated in polymer melts without added compatibilizers, lamellar mesostructured silicates and aluminosilicates with covalently attached hexadecyl functional groups (C_{16}-LMS and C_{16}-LMAS, respectively) were prepared by sol–gel syntheses and their structures were characterized. Based on XRD and TEM data, lamellar products with layer spacings of 4.8–4.9 nm were obtained between room temperature and 60 °C (C_{16}-LMS) or 70 °C (C_{16}-LMAS). The degree of condensation of the aluminosilicate layers increased at the higher synthesis temperatures. Attachment of organic groups to the inorganic sheets was confirmed by ^{29}Si solid state MAS NMR and IR spectroscopy. The sheets of C_{16}-LMS consisted of single or double layers of tetrahedral silicate groups, each attached to a hexadecyl chain. C_{16}-LMAS was composed of pyrophyllite-like layers (Si:Al = 2) with an octahedral aluminum layer sandwiched between two tetrahedral silicate layers and hexadecyl surface groups. Tetrahedral aluminum sites were also present. The clay layer spacing could be increased to 5.2 nm by addition of tetraethoxysilanes during the synthesis (C_{16}-SiO_2-LMAS). C_{16}-SiO_2-LMAS was structurally similar to C_{16}-LMAS; however, the presence of additional silicate groups in this structure increased the inorganic layer thickness and introduced further structural disorder.

Keywords: Lamellar mesostructures; Synthetic clays; Aluminosilicates

1. Introduction

Polymer/clay nanocomposites have received much attention lately due to the advantages they can provide over pure polymers or macrocomposites used in industrial applications. Upon intercalation and exfoliation of clay particles by a polymer, such nanocomposites can exhibit reduced permeability and improved mechanical properties, including increased modulus and reduced linear thermal expansion, when compared to their base homopolymers [1–8]. The modulus of these nanocomposites depends strongly on the degree of exfoliation of the clay [9,10]. An aspect ratio of 100 (ratio of length or width to thickness) is a desirable target for improving modulus and reducing permeability [11,12].

Preparing nanocomposites via direct blending of commercial clays into polymer melts can be a challenge due to three major problems. (1) Miscibility is poor between commonly used non-polar polymers and the relatively polar clays that are commercially available. This limits the dispersion of the commercial clays and the degree of exfoliation. Many researchers have focused on using compatibilizers (polymers modified to include polar functional groups) or modifying montmorillonite to improve the clay–polymer miscibility [2,3,13–17]. (2) A second limitation is that most commercial organically modified clays are prepared from natural clays through a cation exchange process, which limits the amount of organic groups that can be inserted into the clay layers and the ability of the clay to be dispersed or exfoliated. In addition, natural impurities

* Corresponding author. Tel.: +1 612 624 1802; fax: +1 612 626 7541.
E-mail address: stein@chem.umn.edu (A. Stein).

0032-3861/$ - see front matter © 2005 Elsevier Ltd. All rights reserved.
doi:10.1016/j.polymer.2005.03.006

remain in the clay, affecting properties of the nanocomposites such as color and magnetic properties. (3) A third limitation is that the melt blending process requires mixing at relatively high temperatures, which together with high shear rates, can lead to loss of the organic modifier, degradation of polymer, and reduced clay aspect ratios [13,14,18,19].

Seeking to overcome current limitations of commercial clays derived from natural clays, we have investigated an approach to form polymer nanocomposites without the need for a compatibilizer in the melt. Compatibility with non-polar polymers is instead provided by organic functional groups that are attached to inorganic layers in new synthetic clays. These lamellar mesostructures are prepared by sol–gel methods combined with surfactant templating. The clays can be used as synthesized, eliminating the cation-exchange process and natural impurities. Syntheses for a number of similar mesostructures with organic interlayer groups have been reported by several groups, a few of whom also prepared polymer–clay nanocomposites from the synthetic clays [20–40].

The lamellar mesostructured silicates (LMS) and aluminosilicates (LMAS) studied here are shown schematically in Fig. 1. The sample named C_{16}-LMS consists of silicate sheets with covalently attached C_{16}-alkyl chains. Because these C_{16}-alkyl chains act as both surfactant and surface modifier, no additional surfactant was required for the templating process. The samples labeled C_{16}-LMAS and C_{16}-SiO_2-LMAS contain additional aluminum groups within the clay sheets, which were expected to improve the layer stiffness. In C_{16}-SiO_2-LMAS, tetraethylorthosilicate (TEOS) was added to the precursor to produce thicker sheets and, in principle, improve the layer stiffness and strength. These synthetic functionalized clays have large interlayer spacings, and the organic surface groups may act as compatibilizers for blending with non-polar polymers. The surface groups were expected to improve polymer–clay interactions, miscibility, and degree of intercalation/exfoliation in non-polar polymers.

In this paper, we report the syntheses and structures of the synthetic clays. The synthesis conditions were chosen to obtain a lamellar phase and to optimize the degree of condensation and the thermal stability of the synthetic clays.

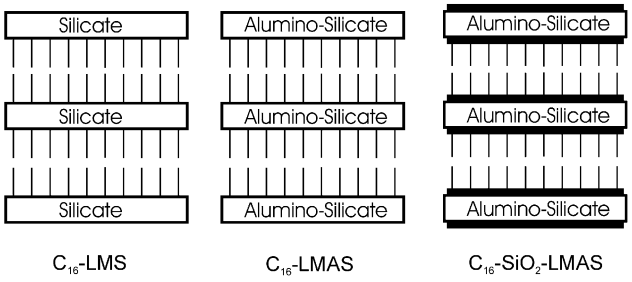

Fig. 1. Schematic structures of the lamellar synthetic clays studied. The rectangular blocks refer to silicate or aluminosilicate layers and the vertical lines to covalently attached hexadecyl groups.

Rheological properties of the clays dispersed in organic solvents and in PS will be reported separately [41].

2. Experimental section

2.1. Materials

Aluminum chloride hexahydrate ($AlCl_3 \cdot 6H_2O$), tetraethyl orthosilicate (TEOS), hydrochloric acid (37 wt%), and sodium hydroxide (NaOH) from Aldrich, hexadecyltrimethoxysilane (HDTMOS) from Gelest, and ethanol (200 proof) from AAPER Alcohol and Chemical Co. were used as received.

2.2. C_{16}-LMS synthesis

HDTMOS and TEOS were combined and stirred for 10–15 min or sonicated in a glass vial to ensure the homogeneity of the solution. The HDTMOS–TEOS mixture was then added to an aqueous HCl solution and permitted to react for 1.5 h at room temperature (RT) and for 1.5 h at 60 °C with rapid stirring. Table 1 lists the mole ratios of reactants. Following the 3 h reaction time, the products were filtered and rinsed repeatedly with distilled water. The products were then allowed to dry for a period of at least 24 h under ambient conditions. Typical amounts of the reactants were: 6.3 g HDTMOS: 3.5 g TEOS: 20.5 g HCl: 60.0 g H_2O.

2.3. C_{16}-LMAS synthesis

Typically, 0.2 M $AlCl_3 \cdot 6H_2O$ in ethanol was hydrolyzed via titration with 0.5 M NaOH solution until a pH of 3.7 was achieved. An equal volume of a 0.4 M HDTMOS solution in ethanol was added to the aluminum solution with stirring over a 15 min period. The mixture was then titrated with a 0.5 M NaOH solution until a pH of 6.5–7.0 was achieved in order to avoid leaching and loss of Al during product washing. More white solids precipitated with additional titration. The solution was stirred rapidly for a designated period of time at the temperature listed in Table 1. When the synthesis was performed at an elevated temperature, the solution was allowed to react at RT for 30–60 min before heat was applied. If a temperature of 100 °C or higher was required, the mixture was loaded into a Teflon-lined autoclave and heated without stirring in an oven. The white solid products were filtered and rinsed repeatedly with distilled water. The products were allowed to dry overnight under ambient conditions.

2.4. C_{16}-SiO_2-LMAS synthesis

In general, the procedure was the same as for the C_{16}-LMAS synthesis described above, except that varying amounts of TEOS were added to the HDTMOS solution,

Table 1
Typical conditions for syntheses of functionalized clays and product phases

Sample	HDTMOS (mol)	$AlCl_3 \cdot 6H_2O$ (mol)	NaOH or HCl (mol)	TEOS (mol)	H_2O (mol)	EtOH (mol)	Reaction time (h) and temperature (°C)	Layer spacing of lamellar phase (nm)
C_{16}-LMS	1.00	–	11.6 HCl	0.934	224	–	1 h RT, 1 h 60 °C	4.8
C_{16}-LMAS, RT	1.00	0.500	1.61 NaOH	–	278	77.5	24 h, 25 °C	4.9
C_{16}-LMAS, 70 °C	1.00	0.500	1.74 NaOH	–	192	77.3	24 h, 70 °C	4.9
C_{16}-SiO_2-LMAS, 70 °C	1.00	0.719	2.59 NaOH	0.439	286	113	24 h, 70 °C	5.2

and this solution was sonicated before being transferred to the aluminum solution. Phase morphologies were investigated at temperatures ranging from RT to 150 °C. Typical mole ratios of reagents and solvents leading to lamellar products are presented in Table 1.

2.5. Characterization

Elemental analyses for C and H were performed by Atlantic Microlabs Inc., Norcross, GA, and analyses for Na, Al, and Si by Galbraith Laboratories, Knoxville, TN. The results are listed in Table 2. Powder X-ray diffraction (XRD) patterns were recorded using a Siemens D-5005 wide-angle XRD spectrometer with Cu K_α radiation, operating at 40 kV and 45 mA. In a typical sample preparation, the powdered materials were placed in quartz cells with dimensions of $0.083'' \times 0.24'' \times 1.05''$. Thermogravimetric analyses (TGA) and differential scanning calorimetry (DSC) were performed in a nitrogen atmosphere using a Netzsch STA 409 PC thermal analyzer. The samples were heated from 25 to 1000 °C at a heating rate of 15 °C/min.

Transmission electron microscopy (TEM) images were recorded digitally using a Jeol 1210 microscope operating at 120 keV. Samples for TEM were prepared by sonicating materials in absolute ethanol for 5 min, and depositing 2–3 drops of the suspension on a holey carbon grid. The samples were allowed to dry at least 30 min before imaging. Scanning electron microscopy (SEM) was performed on the air-dried powder samples using a Jeol 6500 microscope. Samples were dusted on an adhesive conductive carbon disc attached to an aluminum mount. All samples were then coated with 9 nm of Pt. Fourier transform infrared (FT-IR) spectra were obtained with a Nicolet Magna FT-IR 760 spectrometer from samples prepared in a KBr matrix and referenced against a KBr background.

Silicon-29 solid state nuclear magnetic resonance (NMR) spectra were measured using a Bruker ASX-400 spectrometer which includes a 9.4 T magnet (^{29}Si: 79.49 MHz). The ^{29}Si spectra were measured using a single pulse experiment (90° pulse width: 5.5 or 6.0 μs, spinning rate: 5.0 kHz, recycle delay: 150 s) and calibrated using tetrakistrimethylsilane (set to −9.83 ppm relative to tetramethylsilane) as a secondary standard. The ^{27}Al MAS-NMR spectra were measured using a Bruker Avance 400 spectrometer which includes a 9.4 T magnet (^{27}Al: 104.3 MHz). The ^{27}Al spectra were measured using a single pulse experiment (90° pulse width: 2.5 μs, spinning rate: 10.0 kHz, recycle delay: 1.0 s) and calibrated using 1.0 M $AlCl_3$ (0 ppm) as an external reference. Peak deconvolution and curve fitting were performed for the ^{27}Al MAS-NMR spectra using identical conditions for all samples.

3. Results and discussion

3.1. Influence of synthesis conditions on structures of functionalized clays

Syntheses of C_{16}-LMS, the hexadecyl-functionalized

Table 2
Elemental compositions of the synthetic clays

Sample	C (wt%)	H (wt%)	Na (wt%)	Si (wt%)	Al (wt%)	Si:Al (mole ratio)	Inorganic content (wt%)[a]
C_{16}-LMS	66.1	11.8	Trace (< 98 ppm)	10.7[b]	–	–	23.3
C_{16}-LMAS, RT	58.9	10.9	nd	nd	nd	nd	26.3
C_{16}-LMAS, 70 °C	59.8	10.7	1.17	8.22	4.06	1.94	30.3
C_{16}-SiO_2-LMAS, 70 °C	58.2	10.8	2.51	10.5	4.93	2.05	36.3

nd, not determined.
[a] Obtained by TGA analysis, based on remaining mass after heating to 1000 °C.
[b] Calculated by difference from C, H, Na measurements, and using the relative T^1, T^2, T^3 ratios from ^{29}Si NMR measurements.

mesostructured silicates, were attempted within a temperature range from RT to 150 °C for 1–48 h at different precursor ratios. White products were obtained in all cases. Only disordered mesophases with a single low-angle XRD reflection peak were observed for samples prepared at 70 °C, and no XRD reflections were seen for samples prepared at 100 °C or higher. At RT a lamellar phase formed within 3 h, but became disordered at longer reaction times. The most ordered lamellar phase was found when C_{16}-LMS was synthesized at RT for 1.5 h followed by 60 °C for another 1.5 h with the reagent ratio presented in Table 1. The XRD pattern for this sample showed three reflections corresponding to a lamellar phase with d_{001}, d_{002}, and d_{003} spacings of 4.8, 2.4 and 1.6 nm, respectively (Fig. 2). C_{16}-LMS may be compared with MCM-50, a lamellar mesostructured silicate, originally reported by Mobil Corporation [42–44]. MCM-50 consists of 1 nm thick amorphous silica layers separated by cationic surfactant layers (e.g. the C_{16}^{+} surfactant, hexadecyltrimethyl ammonium bromide), which are not covalently attached to the clay sheets. In MCM-50 the C_{16}^{+} surfactant molecules form interdigitating bilayers between silica sheets, resulting in a layer spacing of 3.6 nm [42–44]. In contrast, the C_{16} groups in C_{16}-LMS are covalently attached to the inorganic layers. A value of 4.8 nm for the first order reflection d_{001} implies that the hexadecyl groups are organized into lamellar bilayers since the d_{001} spacing is approximately equal to the length of two hexadecyl groups and the thickness of the silicate layer [21].

The sol–gel synthesis of C_{16}-LMAS was analogous to that reported by Ukrainczyk et al. [21,22], except that a longer alkyl chain was employed in the current study and different synthesis conditions were required to optimize the mesostructures for nanocomposite applications. Product compositions had been reported to be close to $(RSi)_4Al_2O_8(OH)_2$ [21,22]. With a Si:Al ratio of 2:1, silicate layers are expected to be neutral. This ratio was chosen for the current work, as non-polar polymers were targeted for nanocomposite preparations. Before addition of HDTMOS, the reaction mixture was initially titrated to a pH of 3.7 to hydroxylate the aluminum ions. Following hydrolysis and condensation of the alkoxide, titration was terminated at pH 6.5–7 to avoid leaching and loss of Al when washing the products. Titration needed to be carried out slowly to prevent formation of a greasy or oily product. The most ordered lamellar phase, based on intensities and sharpness of XRD reflections, was obtained by heating the reaction mixture at 70 °C for 24 h. Above 100 °C, a disordered mesophase was obtained with only one reflection peak in the XRD pattern. The XRD patterns for the RT and 70 °C samples both showed three low-angle reflection peaks (Fig. 2). A value of 4.9 nm for the first order reflection d_{001} suggested that the hexadecyl groups were organized into lamellar bilayers, as they were in C_{16}-LMS. The layer spacing was consistent with extrapolations from aluminum silsesquioxanes with C_8- and C_{12}-alkyl chains reported to produce layers spacings of 2.5 and 3.8 nm, respectively, for bilayer arrangements [21,22]. A weak XRD reflection was observed at 0.42 nm; it was sharper than reflections typically seen for amorphous silica. A reflection at this spacing has previously been associated with hydrocarbon chains that are oriented perpendicular to the bilayers formed by the hydrocarbons [45]. Similar reasoning may be applied to the current system, and is consistent with the observed clay layer spacings. The layer spacing did not increase with longer reaction times. However, the lamellar phase became less ordered after 48 h based on the broadening of the first order reflection.

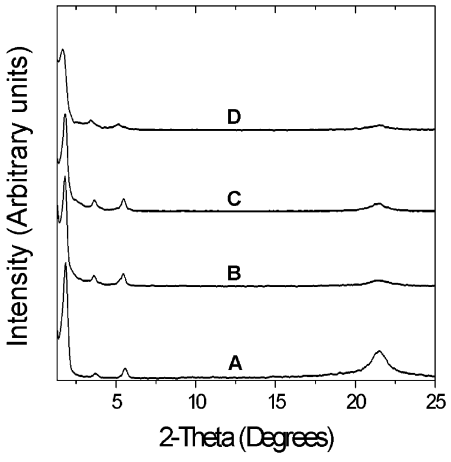

Fig. 2. XRD patterns of the synthetic clays: (A) C_{16}-LMS, (B) C_{16}-LMAS RT, (C) C_{16}-LMAS 70 °C, (D) C_{16}-SiO_2-LMAS 70 °C.

In the C_{16}-SiO_2-LMAS system, TEOS was added to the precursor solution in an attempt to increase the thickness and the stiffness of the inorganic layers. Lamellar phases were formed with TEOS:HDTMOS ratios up to 1:2, but at higher TEOS content, the products became amorphous, showing no reflection peak in XRD pattern. Depending on synthesis time and reaction pH, the layer spacing increased to 5.2–6.0 nm. As the surfactant bilayers could not expand any further, the observed layer spacings imply that aluminosilicate sheets were at least 0.3 nm thicker than in samples where no TEOS was added (Fig. 2). The mesostructure became less ordered at 100 °C (one reflection peak), and was disordered at 150 °C (no XRD reflections).

TGA and DSC curves of all clays showed two major events, gradual loss of water above 100 °C and pyrolysis of the alkyl chains beginning at 250 °C, with major weight loss between 300–560 °C. Weight loss associated with surface water and water of condensation followed the order C_{16}-LMAS RT > C_{16}-SiO_2-LMAS 70 °C > C_{16}-LMAS 70 °C > C_{16}-LMS. The relative masses of inorganic material remaining at 1000 °C for all samples are listed in Table 2. Comparing C_{16}-SiO_2-LMAS 70 °C with C_{16}-LMAS 70 °C, the 6 wt% higher remaining mass for the sample prepared with HDTMOS/TEOS mixtures confirmed that the increased layer spacing was due to thicker inorganic layers in this sample. Unless stated otherwise, the analyses and characterization data

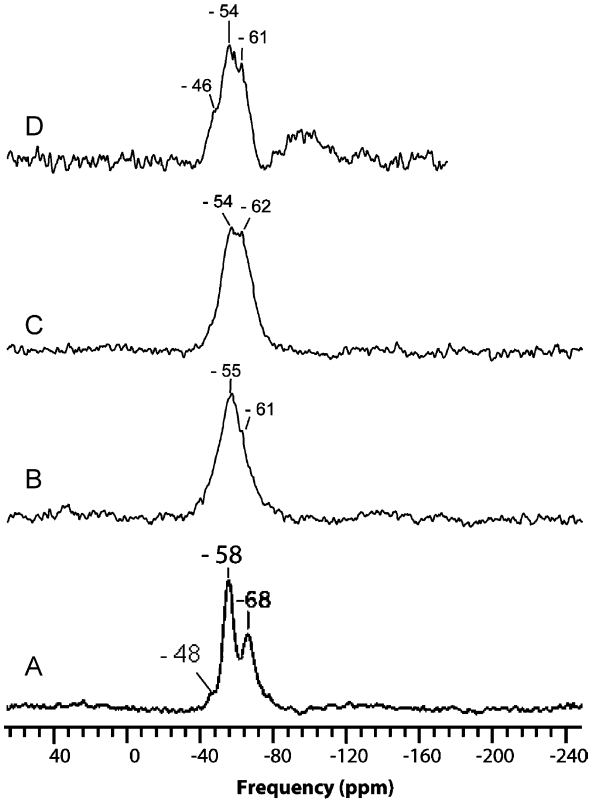

Fig. 3. ^{29}Si MAS NMR spectra of synthetic clays: (A) C_{16}-LMS (B) C_{16}-LMAS RT, (C) C_{16}-LMAS 70 °C, and (D) C_{16}-SiO_2-LMAS 70 °C.

presented subsequently for C_{16}-LMAS and C_{16}-SiO_2-LMAS samples are based on materials synthesized at 70 °C. These materials are denoted as C_{16}-LMAS 70 °C and C_{16}-SiO_2-LMAS 70 °C.

3.2. Structure of clay layers

^{29}Si MAS NMR spectra (Fig. 3) provided information about the silicon environment in the organically functionalized clays and confirmed preservation of the Si–C bonds in the products. One can expect peaks of the type T^m, corresponding to organosiloxane groups $RSi(OSi)_m(OH)_{3-m}$ (m=0–3, R=$C_{16}H_{33}$) and for samples prepared with added TEOS, Q^n peaks associated with siloxane groups, $Q^n=Si(OSi)_n(OH)_{4-n}$ (n=0–4). For C_{16}-LMS, the spectrum (Fig. 3(A) and Table 3) showed 2 distinct peaks: a major T^2 resonance (δ −58 ppm) and a T^3 resonance (δ −68 ppm). A weak shoulder corresponding to T^1 groups (δ −48 ppm) was also observed. Interestingly, no significant Q^n peaks were seen, implying that TEOS was not incorporated in the lamellar product. It should be noted that C_{16}-LMS samples could also be prepared without TEOS. From the NMR data, an approximate formula for C_{16}-LMS is $C_{16}H_{33}\{[SiO_{1.5}]_{0.4}[SiO(OH)]_{0.55}[SiO_{0.5}(OH)_2]_{0.05}\}$, which results in a composition of 67.8 wt% C, 12.0 wt% H, 9.9 wt% Si and 10.3 wt% O, in reasonable agreement with the observed composition (Table 2). Two structural models for C_{16}-LMS, containing only T^n silicate units may be considered. One is based on a single layer structure analogous to the $Na_2Si_2O_5$ structure [46], with alkyl chains occupying the interlayer space. The other model, shown in Fig. 4(A), is derived from a double layer structure similar to that in $CaAl_2Si_2O_8$ [47], but with only Si as tetrahedral atoms and resulting neutral layers separated by alkyl chains. In these two models the inorganic layers are ca. 0.5–0.6 nm thick. ^{29}Si MAS NMR data and chemical analyses are consistent with both models, so that we were unable to distinguish between them. Some disorder in the layers was introduced by terminal hydroxyl groups, which were not shown in Fig. 4(A).

Upon introduction of aluminum into the synthetic clays, the T^2 and T^3 resonances shifted downfield by 2–7 ppm and the envelope of resonances was less well resolved. In clay minerals, a downfield shift of ca. 5 ppm is observed when one Si neighbor is replaced by Al at a tetrahedral Si site (Q^4[1Al]) [48,49], and similar substitutions are likely in C_{16}-LMAS with a Si:Al ratio of approximately 2. Based on curve resolution of the bands (Table 3), the degree of condensation increased in the C_{16}-LMAS sample synthesized at 70 °C, compared to the sample prepared at room temperature. The absence of Q^n peaks in these spectra confirmed that hexadecyl groups were not cleaved from the silicate framework.

In the spectrum of C_{16}-SiO_2-LMAS (Fig. 3(D)), both T^m and Q^n peaks were observed due to condensation of HDTMOS and TEOS in the material. The intensity ratio of T^m and Q^n peaks approximated that of the precursor ratio in the reactant mixture. The relatively broad envelope in the

Table 3
^{29}Si-NMR analysis of the synthetic clays

Sample	Peak position (ppm) and relative amount (%)			
	T^1	T^2	T^3	Q^3
C_{16}-LMS, 1 h RT and 1 h 60 °C	−47.5 (5%)	−57.5 (55%)	−68 (40%)	–
C_{16}-LMAS, RT	−48.9 (28%)	−55.3 (55%)	−61.4 (17%)	–
C_{16}-LMAS, 70 °C	−44.8 (5%)	−54.2 (66%)	−61.6 (29%)	–
C_{16}-SiO_2-LMAS, 70 °C	−46.1 (13%)	−54.0 (45%)	−61.2 (17%)	−79 to −93 (24%)

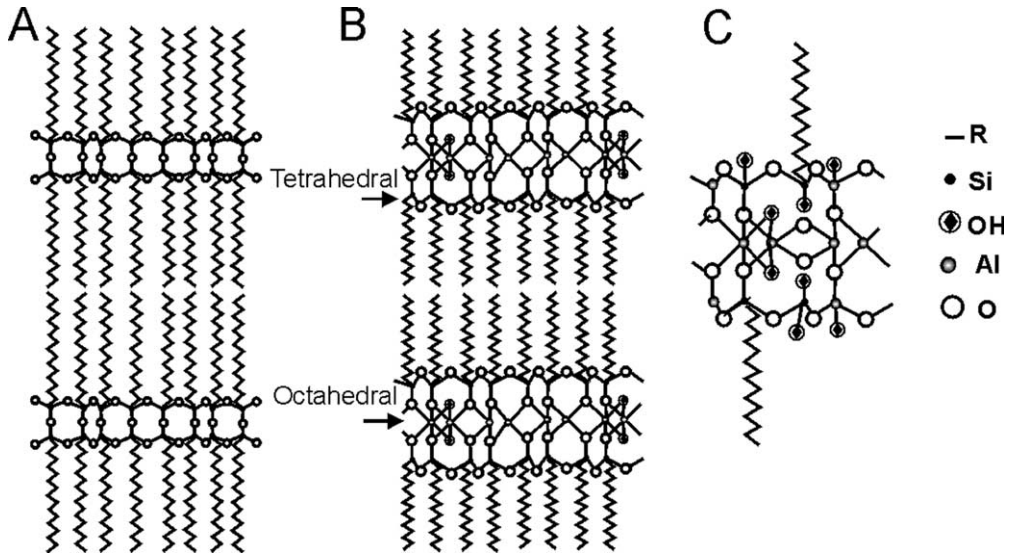

Fig. 4. Proposed schematic structures of the functionalized clays. Two possible structures for C_{16}-LMS include a single layer structure and a double layer structure which is shown in (A). The proposed structure of C_{16}-LMAS (B) is modeled after Ukrainczyk et al. [20,21] with both tetrahedral and octahedral Al present in the octahedral layer. In C_{16}-SiO_2-LMAS (C) additional silicate groups without alkyl chains are present and tetrahedral Al is likely to occupy some of the sites in tetrahedral layers. Terminal hydroxyl groups on tetrahedral Si are not explicitly shown in (A) or (B), but they are present. The alkyl chains in the diagram are schematic; no information about trans-/cis- configuration is implied.

Q^n region may contain contributions from Q^3 with Si connected to 0 or 1 Al (δ −100 to −86 ppm) and Q^4 connected to 0–3 Al (δ −110 to −90 ppm) [49]. The T^2/T^3 ratio was greater in this sample than in the one prepared without TEOS at the same temperature, indicating a lower degree of condensation for the organosilicate groups and a larger fraction of available hydroxyl groups in the material (Table 3). This was consistent with the observation that C_{16}-SiO_2-LMAS products were more hydrophilic than C_{16}-LMAS products.

To discuss the local environment of Al atoms in the clay layers, it is useful to consider the layer model proposed by Ukrainczyk et al., which is based on the pyrophyllite structure [21,22]. A schematic structure, modified for the current LMAS systems, is shown in Fig. 4(B). In the 2:1 pyrophyllite structure, Al is octahedrally coordinated in the central layer. In previously reported aluminum silsesquioxanes with C_{12}-alkyl chains, Al was actually found to be 4-, 5-, and 6-coordinate. Oxygen-deficient, 4- and 5-coordinate Al was believed to be located in the octahedral layer [21, 22]. Al substitution in the tetrahedral layers was deemed less likely. Because of the similar chemistry used for the LMAS systems here, one would also expect incorporation of fully coordinated and oxygen-deficient aluminum in an octahedral layer. The ^{27}Al MAS-NMR spectra of C_{16}-LMAS RT, C_{16}-LMAS 70 °C, and C_{16}-SiO_2-LMAS 70 °C (Fig. 5) all showed resonances corresponding to 4-coordinate Al (δ 56.2–55.5 ppm) and 6-coordinate Al (δ 6.5–3.8 ppm). The ratios of tetrahedral Al (Al_{Td}) to octahedral Al (Al_{Oh}) obtained by deconvolution changed when TEOS was added to the synthesis mixture. For C_{16}-SiO_2-LMAS 70 °C this ratio was 3 Al_{Td}:1 Al_{Oh}, whereas for C_{16}-LMAS prepared at 70 °C or RT, it was only 1.4 Al_{Td}:1 Al_{Oh}. It is possible that some tetrahedral aluminum in C_{16}-SiO_2-LMAS was associated with silicon in a non-octahedral layer. The constant relative peak intensities for C_{16}-LMAS at RT and 70 °C indicated that changing the reaction temperature did not alter the coordination of Al. However, judging from narrower relative peak widths, Al became more ordered after the higher temperature treatment. In both, C_{16}-LMAS and C_{16}-SiO_2-LMAS samples, the Si:Al mole ratio was close to 2, i.e. unchanged from the synthesis mixture. Although for a perfect pyrophyllite-type structure this ratio should result in neutral clay layers, small amounts of sodium

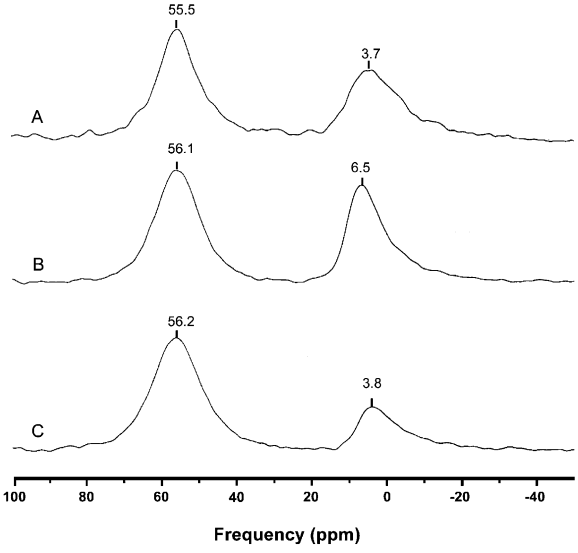

Fig. 5. ^{27}Al MAS NMR spectra of synthetic clays: (A) C_{16}-LMAS RT, (B) C_{16}-LMAS 70 °C, and (C) C_{16}-SiO_2-LMAS 70 °C.

ions were observed in both C_{16}-LMAS and C_{16}-SiO_2-LMAS (Table 2). These cations are likely to balance the charge arising from structural imperfections, which are more significant in the latter materials. The amount of aluminum was almost the same for the two alumino-silicates (Table 2).

Structural formulas for C_{16}-LMAS and C_{16}-SiO_2-LMAS were calculated based on elemental analysis (Table 2) while assuming an ideal pyrophyllite composition where every silicon atom is bonded to a hexadecyl group. The calculated formula for C_{16}-LAMS is $(C_{16}H_{33})_{2.1}Si_{1.94}Al_{1.0}O_{6.65}(OH)_{0.9}$. This corresponds to a distribution of 59.6 wt% C, 10.5 wt% H, 8.05 wt% Si, 3.98 wt% Al, and 17.9 wt% O. The calculated formula for C_{16}-SiO_2-LMAS is $(C_{16}H_{33})_{1.65}Si_{2.03}Al_{1.0}O_{3.32}(OH)_{3.75}$. This corresponds to a distribution of 52.1 wt% C, 9.7 wt% H, 9.35 wt% Si, 4.42 wt% Al, and 18.6 wt% O. The structural formula of C_{16}-SiO_2-LMAS indicates that it contains more hydroxyl groups thatn C_{16}-LMAS. This agrees with NMR analysis and observations of increased hydrophilicity of C_{16}-SiO_2LMAS. A proposed model of the layer structures in C_{16}-SiO_2-LMAS is shown in Fig. 4(C).

FT-IR spectra corroborated some of the conclusions drawn from solid state NMR. Absorptions originating from hexadecyl groups were observed at 2918 and 2850 cm^{-1} (νCH_2), 1467 cm^{-1} (δCH_2), 721 and 685 cm^{-1}(ρCH_2). Absorptions at 1068 and 1100 cm^{-1} corresponding to Si–O stretching vibrations of silicate tetrahedra fell in the typical range for sheet structures with one terminal oxygen [50,51]. Broad absorption bands centered around 3400 cm^{-1} were due to O–H stretching of terminal hydroxyl groups that were hydrogen-bonded to each other and to surface water. The intensity of this absorption was higher in C_{16}-LMAS prepared at RT than at 70 °C, consistent with

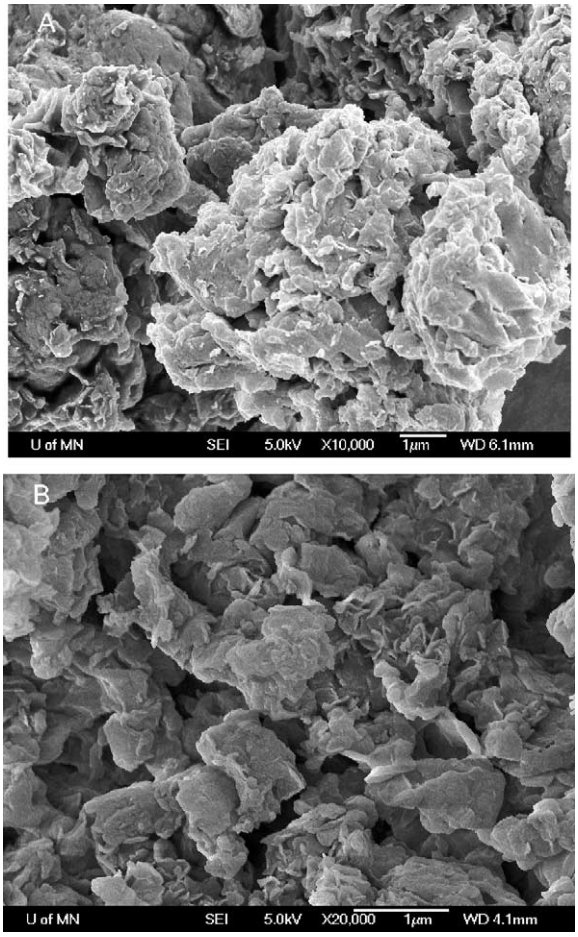

Fig. 6. SEM micrographs of (A) C_{16}-LMS, and (B) C_{16}-SiO_2-LMAS.

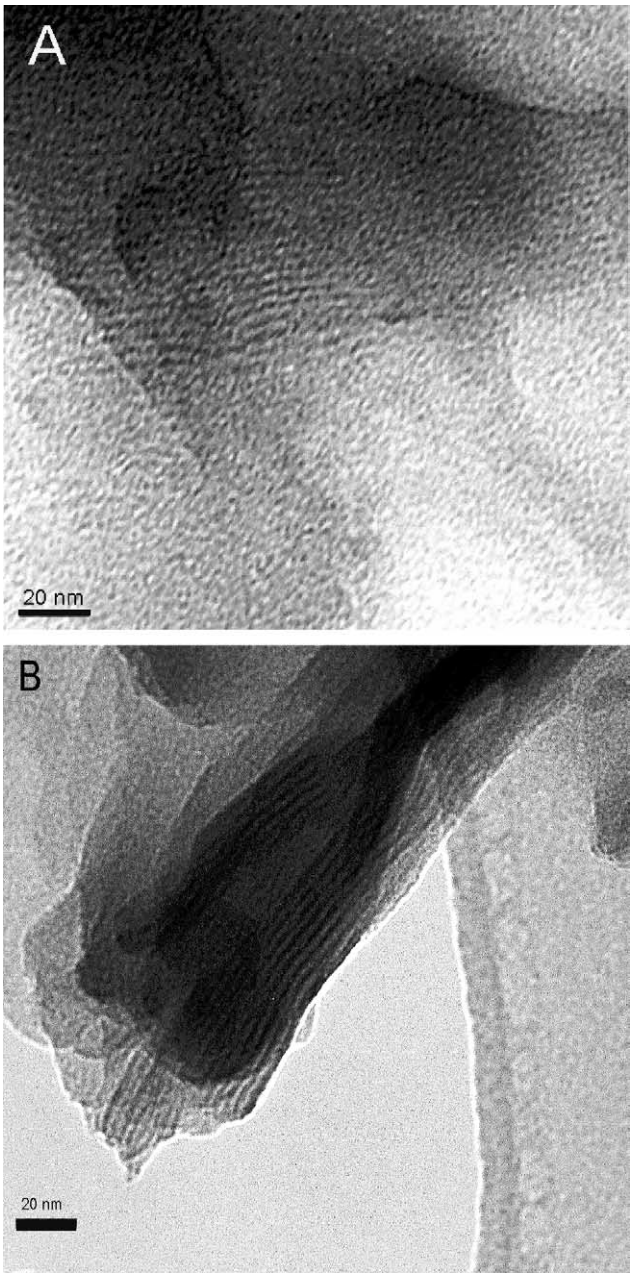

Fig. 7. TEM micrographs of (A) C_{16}-LMS and (B) C_{16}-SiO_2-LMAS 70 °C showing the layer morphology of the platelet stacks (dark lines) which are separated by surfactant layers (lighter lines).

data from ^{29}Si MAS NMR spectra, which suggested a greater degree of condensation at the higher temperature. For different clay compositions prepared between 60–70 °C, the intensity of the –OH stretching absorption decreased in the order C_{16}-LMS > C_{16}-SiO_2-LMAS > C_{16}-LMAS. The variations in hydroxyl content suggest that the hydrophobic nature of these clays (and therefore the extent of clay–polymer interactions in nanocomposites) can be modified by varying the synthesis temperature and the TEOS content in the synthesis mixture.

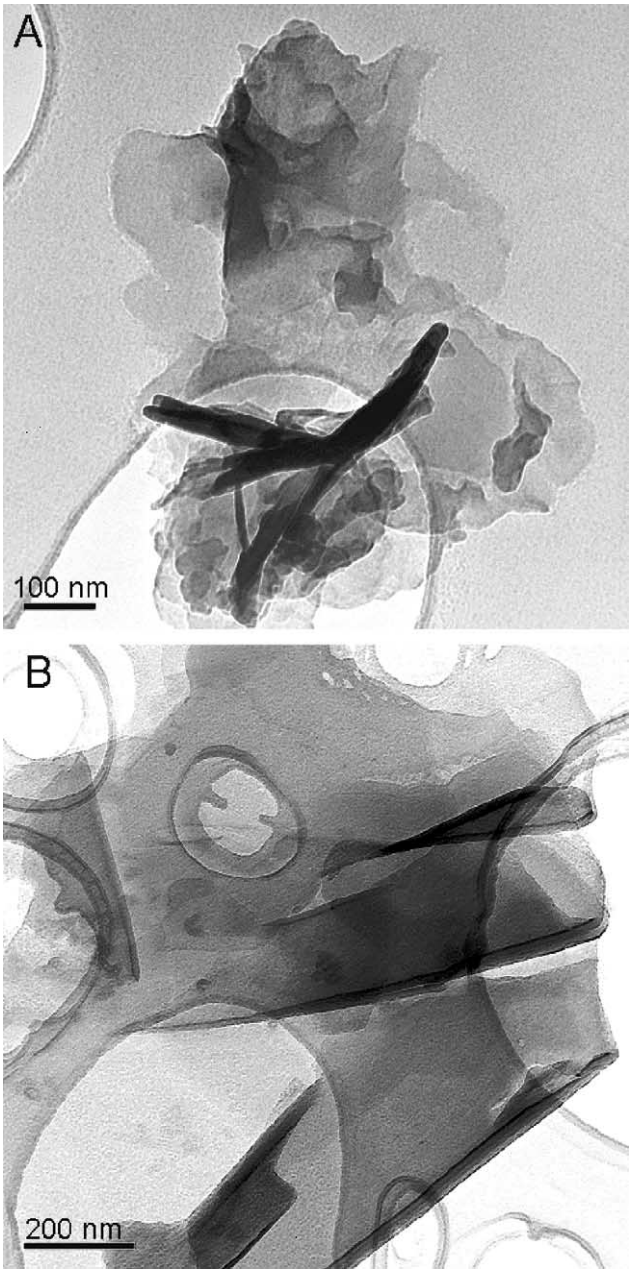

Fig. 8. TEM micrographs showing the sheet-like morphologies of (A) C_{16}-LMAS RT and (B) C_{16}-LMAS 70 °C.

3.3. Morphology and particle size of synthetic clays

SEM images of C_{16}-LMS showed that particles were composed of aggregated plates (Fig. 6(A)). Due to the cauliflower-like aggregation, it was difficult to determine dimensions of individual plates. SEM images of C_{16}-LMAS and C_{16}-SiO_2-LMAS are similar and presented in Fig. 6(B). The Al-containing synthetic clays were also composed of aggregated, plate-like particles with typical sizes ranging from 0.9–1.3 μm (edge-to-edge) for C_{16}-LMAS and 0.7–0.9 μm (edge-to-edge) for C_{16}-SiO_2-LMAS, although some particles were significantly larger. Some C_{16}-SiO_2-LMAS particles were curled at the edges, suggesting that sheets were more distorted in this sample. The TEM micrographs of cross-sections of C_{16}-LMS (Fig. 7(A)) and C_{16}-SiO_2-LMAS (Fig. 7(B)) show dark and light parallel lines corresponding to alternating inorganic and surfactant layers at 4–5 nm intervals, in agreement with the d_{001} XRD spacings for these samples. TEM cross-sections of C_{16}-LMAS (not shown) were similar. A comparison of TEM images for C_{16}-SiO_2-LMAS and C_{16}-LMAS showed thicker aluminosilicate layers in the former (average ca. 1.9 nm, compared to 0.9 nm). Even though one must be careful with thickness measurements from the TEM images, the trend is consistent with the larger layer spacings observed by XRD for C_{16}-SiO_2-LMAS. TEM images of C_{16}-LMAS prepared at RT and at 70 °C (Fig. 8) show thin layers in the plane of the image. Typical sheet sizes were larger for the sample prepared at 70 °C compared to the RT sample. Some more elongated particles were also visible. At present it is not clear whether these consist of rolled-up sheets, which have been observed, for example, in layered niobates [52]. Some TEM micrographs showed large stacks of platelets, which appear dark and are flexible enough to curl at the edges. This is typical for a smectic clay structure [27].

4. Conclusions

Three synthetic clays with hexadecyl surface groups (C_{16}-LMS, C_{16}-LMAS, and C_{16}-SiO_2-LMAS) were synthesized, each having a lamellar morphology, based on XRD patterns and TEM micrographs. The organic functional groups were attached to the inorganic layers as confirmed by IR and ^{29}Si-NMR spectra. In polymer–clay nanocomposite applications, attachment of the functional groups is significant, as it can modify polymer–clay interactions without permitting surfactant-leaching into the polymer matrix, a process that can lead to poorer mechanical properties of the polymer. The inorganic sheet structures were different in C_{16}-LMS and C_{16}-LMAS. The former consisted of single or double layers of tetrahedral silicates, the latter of pyrophyllite-like layers with an octahedral aluminum layer sandwiched between two tetrahedral silicate layers. It was possible to increase the layer spacing of C_{16}-LMAS by adding TEOS precursor to

form C_{16}-SiO_2-LMAS. The incorporation of TEOS into the inorganic layers was confirmed by ^{29}Si-NMR spectroscopy, based on the presence of Q^n peaks. Since C_{16}-SiO_2-LMAS contained the same 16-carbon alkyl groups as C_{16}-LMAS, the observed increase in layer spacing could be attributed to an increased inorganic sheet thickness, which was confirmed by TEM micrographs and by a higher residual mass of calcined C_{16}-SiO_2-LMAS measured by TGA. The C_{16}-SiO_2-LMAS sample contained more tetrahedral aluminum, and more hydroxyl defects than C_{16}-LMAS, leading to greater disorder and more hydrophilic behavior for the former structure. The degree of condensation and hydrophobic nature of the synthetic clays could be increased by employing higher synthesis temperatures within the range leading to lamellar structures. The structural difference of the sheets can affect their stiffness and other mechanical properties.

The ability to modify the sheet architecture, the surface properties, and the layer spacings of synthetic functionalized clays is expected to benefit applications involving formation of polymer–clay nanocomposites. The larger layer spacings (5–6 nm) compared to commercial organoclays (2–3 nm) may facilitate intercalation/exfoliation of the synthetic clay layers because interactions between inorganic sheets are reduced. The synthetic clays prepared in this study are nearly neutral, and surface polarity is decreased by alkyl surface groups. One may therefore expect stronger interactions of these clays with non-polar polymers compared to organoclays prepared from natural ionic clays (e.g. montmorillonite). By choosing an appropriate functional group and sheet structure, a synthetic clay may be optimized for blending with a particular polymer or solvent system. The interactions of the synthetic clays with selected solvents and PS melts will be discussed in a separate paper [41].

Acknowledgements

This research was supported by General Motors (GM), and the Industrial Partnership for Research in Interfacial and Materials Engineering (IPRIME) at the University of Minnesota and by the MRSEC program of the NSF (Grant No. DMR-0212302). We acknowledge Charlene Hayden at GM research for obtaining ^{27}Al MAS NMR spectra.

References

[1] Alexandre M, Dubois P. Mat Sci Eng 2000;28:1–63.
[2] Kato M, Usuki A, Okada A. J Appl Polym Sci 1997;63:137–9.
[3] Karger-Kocsis J. Polypropylene: structure, blends, and composites. London: Chapman and Hall; 1995.
[4] Vaia RV, Teukolsky RK, Giannelis EP. Chem Mater 1994;6:1017–22.
[5] Lan T, Kaviratna PD, Pinnavaia TJ. Chem Mater 1994;6:573–5.
[6] Haraguchi K, Takehisa T, Fan S. Macromolecules 2002;35:10162–71.
[7] Choi YS, Wang KH, Xu M, Chung IJ. Chem Mater 2002;14:2936–9.
[8] Pinnavaia TJ, Beall GW. Polymer–clay nanocomposites. New York: Wiley; 2001.
[9] Brune DA, Bicerano J. Polymer 2002;43:369–87.
[10] Vu YT, Mark JE, Pham LH, Engelhardt M. J Appl Polym Sci 2001;82:1391–403.
[11] Dolgovskij MK, Fasulo PD, Lortie F, Macosko CW, Ottaviani RA, Rodgers WR. Effect of mixer type on exfoliation of polypropylene nanocomposites. ANTEC 2003;2255–9.
[12] Fredrickson GH, Bicerano J. J Chem Phys 1999;110:2181–8.
[13] Cho JW, Paul DR. Polymer 2001;42:1083–94.
[14] Dennis HR, Hunter DL, Chang D, Kim S, White JL, Cho JW, et al. Polymer 2001;42:9513–22.
[15] LeBaron PC, Wang Z, Pinnavaia TJ. Appl Clay Sci 1999;15:11–29.
[16] Wolf D, Fuchs A, Wagenknecht U, Kretzschmar B, Jehnichen D, Haussler L. Nanocomposites of polyolefins clay hybrids. Lyon-Villeurbanne: Eurofiller's 99; 1999: p. 6–9.
[17] Kato M, Usuki A, Okada A. J Appl Polym Sci 1997;66:1781–5.
[18] Fornes TD, Yoon PJ, Keskkula H, Paul DR. Polymer 2001;42:9929–40.
[19] Lincoln DM, Vaia RA, Wang ZG, Hsiao BS. Polymer 2001;42:1621–31.
[20] Huo Q, Margolese DI, Stucky GD. Chem Mater 1996;8:1147–60.
[21] Ukrainczyk L, Bellmann RA, Anderson AB. J Phys Chem B 1997;101:531–9.
[22] Ukrainczyk L, Bellmann RA, Smith KA, Boyd JE. Mat Res Soc Symp 1997;457:519–24.
[23] Burkett SL, Sims SD, Mann S. Chem Commun 1996;1367.
[24] Sims SD, Burkett SL, Mann S. Mat Res Soc Symp Proc 1996;431:77–82.
[25] Jaber M, Miehe-Brendle J, Le Dred R. J Mater Sci 2004;39:1489–90.
[26] Parikh AN, Schivley MA, Koo E, Seshadri K, Aurentz D, Mueller K, et al. J Am Chem Soc 1997;119:3135–43.
[27] Carrado KA, Xu L, Csencsits R, Muntean JV. Chem Mater 2001;13:3766–73.
[28] Fujimoto Y, Shimojima A, Kuroda K. Chem Mater 2003;15:4768–74.
[29] Jadhav SM, Burkett SL. Abstracts of papers, 224th ACS National Meeting, Boston, MA, United States, August 18–22, 2002, INOR-505; 2002.
[30] Jadhav SM, Burkett SL. Abstracts of papers, 225th ACS National Meeting, New Orleans, LA, United States, March 23–27, 2003, MTLS-022; 2003.
[31] Mochizuki D, Shimojima A, Kuroda K. J Am Chem Soc 2002;124:12082–3.
[32] Schmidt DF, Qian G, Giannelis EP. Book of abstracts, 219th ACS National Meeting, San Francisco, CA, March 26–30, 2000, PMSE-080; 2000.
[33] Schmidt DF, Qian G, Giannelis EP. Polym Mater Sci Eng 2000;82:215–6.
[34] Shimojima A, Kuroda K. Chem Lett 2000;11:1310–1.
[35] Shimojima A, Kuroda K. Langmuir 2002;18:1144–9.
[36] Shimojima A, Sugahara Y, Kuroda K. Bull Chem Soc Jpn 1997;70:2847–53.
[37] Shimojima A, Sugahara Y, Kuroda K. J Am Chem Soc 1998;120:4528–9.
[38] Ogawa M. Langmuir 1997;13:1853–5.
[39] Herrera NN, Letogge J-M, Putaux J-L, David L, Bourgeat-Lami E. Langmuir 2004;20:1564–71.
[40] Singh A, Haghighat R. US Patent No. 6,057,035.
[41] Chastek TT, Stein A, Macosko CW. Polymer 2005, this issue, doi:10.1016/j.polymer.2005.02.062.
[42] Beck JS, Vartuli JC, Roth WJ, Leonowicz ME, Kresge CT, Schmitt KD, McCullen SB, Higgins JB, et al. J Am Chem Soc 1992;114:10834–43.
[43] Kresge CT, Leonowicz ME, Roth WJ, Vartuli JC, Beck JS. Nature 1992;359:710.

[44] Kresge CT, Vartuli JC, Roth WJ, Leonowicz ME, Beck JS, Schmitt KD, McCullen SB, Higgins JB, et al. Sci Technol Cataly 1994;11–19.
[45] Janiak MJ, Small DM, Shipley GG. Biochemistry 1976;15:4575–80.
[46] Pant AK. Acta Cryst 1968;B24:1077–83.
[47] Takeuchi Y, Donnay G. Acta Cryst 1959;12:465–70.
[48] Mehring M. High resolution NMR spectroscopy of solids. 2nd ed. New York: Springer; 1983.
[49] Engelhardt G, Michel D. High-resolution solid-state NMR of silicates and zeolites. Chichester: Wiley; 1987.
[50] Flanigen EM. ACS Monograph 1976;171:80–117.
[51] Nakamoto K. Infrared and Raman spectra of inorganic and coordination compounds. 5th ed. New York: Wiley; 1997.
[52] Saupe GB, Waraksa CC, Kim H-N, Han YJ, Kaschak DM, Skinner DM, et al. Chem Mater 2000;12:1556–62.